Advanced Atomic Force Microscopy:
Exploring Measurements of Local Electric Properties

Application Note

Sergei Magonov, John Alexander
Agilent Technologies

Introduction

In the past two decades Atomic Force Microscopy (AFM)[1] has been recognized as a powerful characterization method of surfaces at small scales and in different environments. In addition to high-resolution visualization of surface morphology and nanoscale structures, AFM microscopes are also broadly applied for examination of mechanical, electromagnetic, optical and other properties. The core of this technology is the measurement and control of force interactions between a minute probe and a sample surface. Practically, such measurements can be performed at a single location and applied for surface imaging with contact or oscillatory techniques. The techniques complement each other yet studies of soft matter are mostly carried out with oscillatory amplitude modulation (AM) mode.[2-3] Despite an expanding penetration of AFM and the related scanning probe microscopy methods into academic and industrial research, a critical analysis of the existing capabilities of this method reveals a number of undeveloped areas that are essential for further progress of the field. We will mention only a few of them. The current efforts towards imaging with true molecular and atomic resolution in different environments benefit from an extension of frequency modulation (FM) mode[4] to measurements in air and under liquid.[5] The improvement of noise characteristics of AFM electronics and the minimization of thermal drift of the microscopes will undoubtedly assist researchers using extremely sharp probes in achieving superior imaging resolution. In the probing of local mechanical and electric properties increasing attention is paid to multi-frequency measurements that offer new capabilities for quantitative analysis. Studies employing multi-frequency measurements in the broad frequency range help avoid cross-talk of topography with mechanical and electric tip-sample force effects and have other advantages. A successful realization of these possibilities simultaneously with improved resolution of imaging and mapping of materials' properties will open new horizons for AFM characterization especially if these applications can be performed in the properly-controlled environments. This goal can be achieved only in direct interplay of instrumentation developments and their practical verification on various samples. This is our vision of advanced AFM and we hope that this paper supports it.

In the commercial scanning probe microscopes made by Agilent Technologies the first steps towards advanced AFM measurements were undertaken with the introduction of the MAC III accessory especially useful for multi-frequency measurements. The MAC III has three dual phase lock-in amplifiers (LIA) converting the AC inputs to amplitude and phase. These digitally-controlled analog LIA have a broad bandwidth (up to 6 MHz) that covers the operation bandwidth of the photodetector employed in the microscope. The auxiliary inputs and drive outputs are accessible through the MAC III signal access box. The software, which is flexible in routing signals back to the microscope controller, supports two servo systems related to these LIA. One LIA is used for AM tracking of sample topography with the probe peak-to-peak amplitude or its X-, Y- vector components used for feedback. The other servo can be applied to electric or mechanical measurements. The third LIA can be used for tuning the operational parameters or for recording various signals (lateral response, torsional signal, harmonics, etc) during measurements. Voltages up to 20 V in DC or in different pulse regimes can be applied to the probe-sample junction as an external stimulus for lithography or other applications.

Electrostatic force effects in AFM

In microscopy, the compositional mapping of heterogeneous materials is based on recognition of dissimilar sample components. In AFM this is achieved by differentiating the probe-sample interactions at the locations with different mechanical (modulus, friction, adhesion, viscoelasticity, etc), magnetic, electric or other properties. Compositional mapping is the compelling industrial application for analysis of multicomponent materials and it will be advanced further as the contrast variations observed in AFM images will be interpreted quantitatively in terms of materials properties. Although the AFM-based mechanical studies are the most explored application area, this paper is focused on studies of local electric behavior of various samples. Both contact and oscillatory techniques are used for AFM-based electric characterization yet we will consider mostly oscillatory AM mode and only in some cases will mention its companion – the FM mode. In the experiment, as the oscillating probe, which initially vibrates at or near its first flexural resonance ω_{mech} with amplitude A_0, approaches the sample, first, it will sense van der Waals forces, which change the tip-sample force gradient and shift the probe resonance to lower-frequencies. In a non-dissipative case, this shift is the only effect changing the amplitude-versus-frequency (A-v-ω) dependence. In AM mode, the amplitude change at ω_{mech} is employed by a feedback loop to keep the tip-sample interaction constant during surface profiling. On further approach toward the sample, the probe comes into intermittent contact and the topography and phase images are collected at set-point amplitude (A_{sp}) chosen by the researcher. For a particular probe and chosen A_0 the tip-sample force can be adjusted by varying A_{sp}. The experiments can be performed either at low tip-sample forces – the condition for a most gentle and high-resolution imaging of surfaces, or at elevated forces – the condition for compositional imaging based on differences of local mechanical properties.[6] In many cases, the phase images obtained at elevated tip-sample forces are most informative for such qualitative analysis of heterogeneous samples. The situation becomes more complicated when the probe behavior is also influenced by electrostatic tip-sample interactions.

In traditional AM studies the electrostatic forces between a conducting probe and a sample surface with local charges manifest themselves in many ways. The amplitude-vs-Z (AvZ) and phase-versus-Z curves will have a signature of long-range electrostatic interactions, which also impact imaging in the non-contact regime. Figures 1A-H illustrate these effects showing the AvZ curve and images taken at different A_{sp} on the surface of a $LiNbO_3$ crystal with Ag particles deposited along a grain boundary. The AvZ curve demonstrates a gradual drop of amplitude at large tip-sample separations. The topography and phase images recorded at A_{sp}, which is chosen along this part of the curve, show that on approach of the probe to the sample, the Ag particles are first detected in the phase image (grey circle). This is due to higher sensitivity of the phase changes to long-range electrostatic forces between the charged Ag particles and the conducting probe. On further approach, the increasing attractive force leads to higher phase contrast, and the similar pattern appears in the topography images (red and green circles). At some probe-sample distance the oscillating tip comes into intermittent contact and the AvZ curve changes from the gradual decline to the abrupt one. At A_{sp} along the steep part of the AvZ curve (blue circle) the topography image distinctively shows a granular morphology of the $LiNbO_3$ surface and the string of Ag particles. The related phase image enhances the edges of the grains similar to the amplitude (error

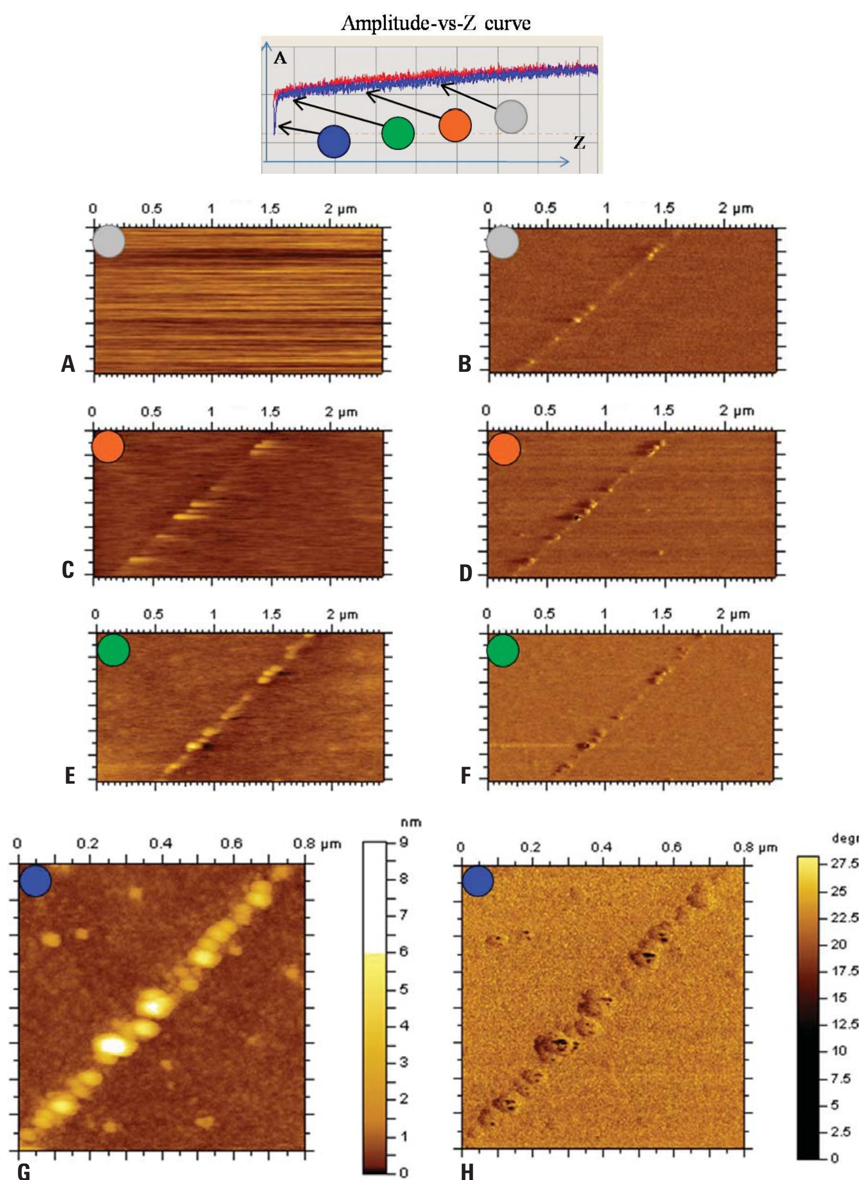

Figure 1A-H. Top – amplitude-versus-distance curve on $LiNbO_3$/Ag surface. The topography (A, C, E) and phase images (B, D, F) at different A_{sp} as marked by color dots.

signal) image indicating the overwhelming contribution of tip-sample mechanical interactions to the image contrast. In other words, in AM mode when the probe behavior is measured at single frequency (ω_{mech}), the electrostatic forces dominate the probe response in the non-contact regime but their effect becomes negligible in the intermittent contact.

The intermittent contact AM imaging of samples with charged locations can be "disturbed" by a voltage applied to a conducting probe as shown in Figures 2A-F. The images of semifluorinated alkane $F(CF_2)_{14}(CH_2)_{20}H$ (further referred as $F_{14}H_{20}$) adsorbates on graphite exhibit strong contrast variations of several domains (one is outlined with a red circle) as the probe voltage is changing. When imaging was performed with a non-biased probe, the domains in the topography image were not distinguishable from their surrounding yet they exhibited different contrast in the phase images. The same locations became pronounced in the topography images once the probe was biased (+3 V and -3 V) with respect to the sample. This observation raises a question regarding true topography measurements in AM. The false topography contrast is often observed in AM studies of smooth heterogeneous surfaces where more adhesive regions are "elevated" compared to less adhesive ones.[7] This effect is a consequence of a shift of the probe resonance frequency by attractive tip-sample interactions. Therefore, a negative charge of the outlined domain can explain its appearance in Figures 2C, 2E. Actually, surface charges might influence the topography measurements even when a regular Si probe is applied. Such probes have some level of conductivity and the surface charge can induce mirror charges in the probe and the related attractive interaction. A compensation of the surface charge effect by a proper voltage applied to the probe will help reveal the precise topography.

Figures 3A-B present another case when a voltage applied to the probe enhances a number of particles in the topography image of thermoplastic vulcanizate – the material, which contains carbon black buried inside a polypropylene and rubber blend. These changes are caused by electrostatic force between the probe and carbon black particles contributing to a conducting percolation network in this composite material. A subtraction of the topography images will show these particles with even higher resolution as

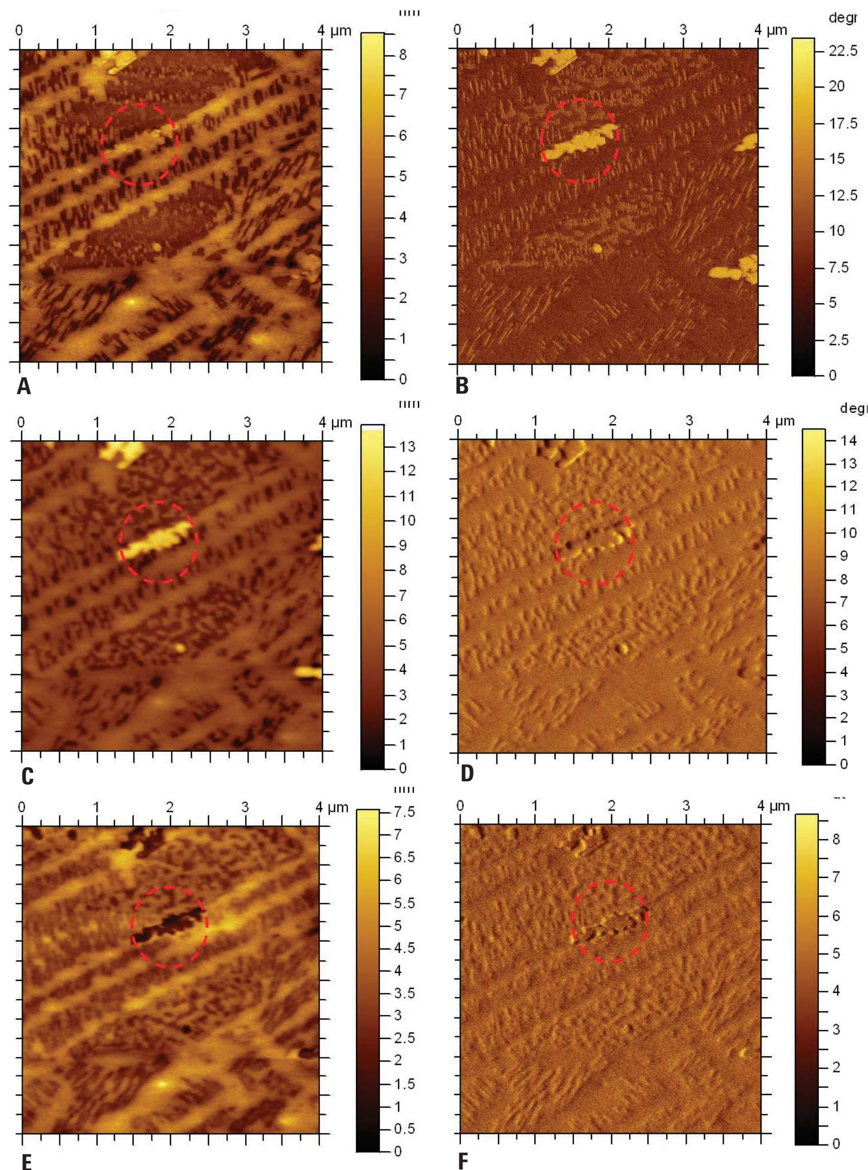

Figure 2A-F. Topography (A, C, E) and phase (B, D, F) images of an adsorbate of semifluorinated alkane $F_{14}H_{20}$ on graphite. The images in (A)-(B) were obtained with a non-biased probe, the images in (C)-(D) were recorded with the bias voltage +3 V and the images in (E)-(F) – with the bias voltage of -3 V.

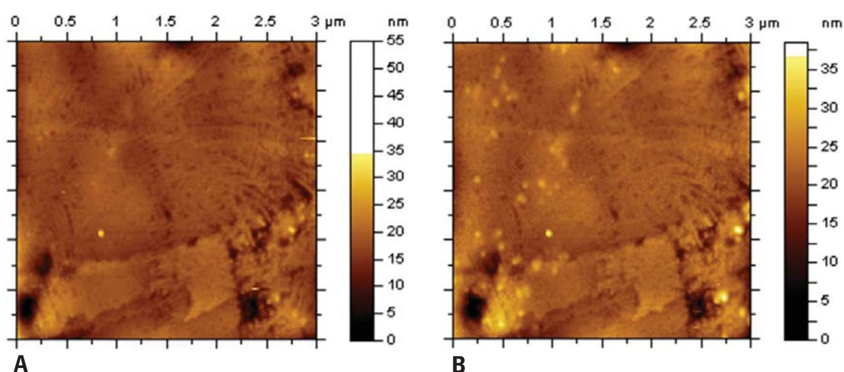

Figure 3A-B. The topography images of thermoplastic vulcanizate obtained with a non-biased probe (A) and with the bias voltage of +3 V.

compared to one of the 2-path electric force microscopy (EFM) enabled by a lift technique.[8] In the latter mode the probe is positioned above the surface and this lowers the EFM resolution. These examples clearly demonstrate that the probe responds simultaneously to the tip-sample mechanical and electrostatic interactions and their separation is the most essential problem of AFM-based electric measurements.

Background on Electric Force Microscopy (EFM) and Kelvin Force microscopy (KFM)

The use of AFM for examination of local electric properties of surfaces was suggested since the advent of this technique. A typical scheme of detection of electrostatic forces includes a conducting probe which is biased with respect to a back electrode or substrate carrying a sample on top. In a simplified form the contribution of electrostatic force is proportional to Ψ^2 and $\frac{\partial c}{\partial z}$, where Ψ – potential difference, C – capacitance and Z – the probe-sample separation.

(1) $F_{elec}(Z) = \frac{1}{2}\,\frac{\partial c}{\partial z}\,\Psi^2$

When DC (U_{DC}) voltage and AC (U_{AC}) voltage at frequency ω, are applied to the probe then the electrostatic force can be expressed as

(2) $F_{elec}(Z) = \frac{1}{2}\,\frac{\partial c}{\partial z}\,[(\varphi - U_{DC} - U_{AC}\sin(\omega t))]^2$,

where φ – surface potential or contact potential difference between the probe and the sample.

This equation can be separated into three components defining the DC and frequency responses:

(3) $F_{DC}(Z) = \frac{1}{2}\,\frac{\partial c}{\partial z}\,(\varphi - U_{DC})^2 + \frac{1}{2}U^2{}_{AC}$

(4) $F_{\omega}(Z) = -\frac{\partial c}{\partial z}\,[(\varphi - U_{DC})U_{AC}\sin(\omega t)]$

(5) $F_{2\omega}(Z) = -\frac{1}{4}\,\frac{\partial c}{\partial z}\,U^2{}_{AC}\cos(2\omega t)$

This set of equations describes the electrostatic force measurements in the capacitor-like set-up. The idea of using two frequencies for simultaneous and independent measurements of surface topography and electrostatic forces was implemented in one of the first AFM applications.[9] In these non-contact experiments, AC voltage was applied to a conducting probe at ω_{elec} and the changes of the probe amplitude at this frequency were detected at different probe-sample separations, which were adjusted by changing A_{sp} at the frequency of mechanical resonance, ω_{mech} (>ω_{elec}). These measurements showed high sensitivity of the applied detection scheme. In the next step, maps of electric properties of a photoresist on a Si substrate and of a working *p-n* junction in a transistor were obtained by recording the amplitude changes at ω_{elec} and $2\omega_{elec}$.[9]

In other experiments during the same time,[10] surface charges, which were made by voltage pulses between a tip and PMMA layer on the Si substrate, were examined in AM mode operating in the non-contact regime (ω_{mech} = 20 kHz). The surface charges have induced the false topography profiles – similar to those demonstrated above in the non-contact and intermittent contact images in Figures 1C, 1D and 2C, 2E, respectively. The AM imaging of the surface charges was further extended by using low-frequency AC voltage (ω_{elec} = 300 Hz) and monitoring the amplitude changes at ω_{elec} and $2\omega_{elec}$.[11] These pioneering measurements of the AFM probe response to electrostatic forces and mapping it over a scanned area defined electric force microscopy (EFM). The extraction of quantitative electric properties from surface maps of amplitude changes at ω_{elec} is a challenging task.[12] The quantitative detection of surface potential was simplified with a null-force method.[13] In this procedure, a combination of DC and AC (at ω_{elec}) voltages was applied to the probe and the DC level is changed until the AC vibration of the probe (at ω_{elec}) is nullified, see equation (4). In first demonstration of the null-force method a voltage map of the precision operational amplifier in a functioning state was made. Later, the null-force method was applied to detection of local contact potential difference (CPD)[14] and this set-up was named Kelvin probe force microscopy (KFM). In addition to EFM and KFM, probing of local electrostatic properties in non-contact mode has been diversified by using the $2\omega_{elec}$ response [see equation (5)] for the feedback mechanism.[15-17] In such a way one can get information regarding the local dielectric constant and its high-frequency dispersion.[15] Simultaneous measurements of sample topography (ω_{mech} = 70 kHz), surface potential (ω_{elec}) and dielectric or polarization response ($2\omega_{elec}$) were performed while the probe was scanning ~ 30 nm above the sample surface.[17] The use of EFM and KFM has increased as they become available in commercial scanning probe microscopes. This happened with the introduction of the lift mode, that makes possible 2-pass EFM and KFM measurements at the single frequency (ω_{mech}). The 2-pass method is a simple separation of the mechanical and electrostatic interactions by switching between the intermittent contact and the non-contact operations. In principle, this switching can be realized by changing A_{sp}. Yet due to thermal drift and other instrumental imperfections the imaging in the non-contact regime where the probe feels only long-range forces is not stable. The problem is solved when in each scan line the probe is raised above the surface only a small height to the non-contact position where the electrostatic response is measured separately from the topography. The tradeoff is the extra time needed for such operation and the remote position of the probe sensing electrostatic forces.

Outlook on EFM and KFM applications

The practical value of EFM and KFM has been established in applications to different materials, ranging from semiconductor structures to biological specimens. In studies of semiconductors and metals, KFM is applied for quantitative measurements of the surface potential of small structures such as thin films, layers, lines, quantum dots and the planar and cross-section dopant profiles. The correlation of the surface potential or CPD data with Fermi level and the influence of surface contamination, oxide coverage and environment on these data are of special concern. The KFM measurements were also made on various small-scale devices including organic thin-film transistors. The mapping of surface potential in the accumulation layer revealed surface potential changes at the film interfaces between the source and drain elements.[18-19] A correlation between surface photovoltage and polymer blend morphology has been examined in polyfluorene-based photodiodes in dark and illuminated conditions.[20] In the bilayer geometry, two polymers, which serve as holes-rich and electrons-rich reservoirs, adopt a complex morphology with domains of different charges. Particularly, low photodiode efficiency was explained by a presence of charged domains caused by steric hindrances to their recombination. The morphology-surface potential relationship was examined in another photovoltaic material – the 100 nm film of an organic blend consisting of soluble fullerene derivative (acceptor) and para-phenylene-vinylidene (PPV)-based polymer on ITO substrate (acceptor).[21] The data were applied for the explanation of different photovoltaic behavior of the films prepared from different solvents.

A dependence of surface potential on molecular order was found in studies of poly-3-methylthiophene at various doping levels.[22] The surface potential was different not only between amorphous and crystalline components but also between individual sectors of crystallites.[23] This invokes a challenging task – the interpretation of surface potential in terms of molecular arrangement, molecular chemical structures and their dimensions. Semifluorinated compounds, which exhibit a strong polar nature due to the dipole at the $–CH_2$-CF_2- bond, are suitable compounds for studying this problem. The KFM images, which were obtained on a mixed monolayer of perfluorodecanoic acid (FC) and arachidic (HC) polyion complexed with (poly(4-methylvinyl pyridinium) iodide, revealed the phase-separation in this material.[24] The surface potential contrast of the components was explained by different strength of dipoles of $C^{\delta+}$- $F^{\delta-}$ and C-H bonds of the FC and HC components. In another example, a micro-contact-printed pattern with alternative domains of alkylsilane $[H_3C(CH_2)_{17}Si(OCH_3)_3]$ - ODS and fluoroalkylsilane $[F_3C(CF_2)_7(CH_2)_2Si(OCH_3)_3]$ - FAS on a Si substrate was prepared as a test structure for KFM.[25] The highest-contrast images, which differentiate the fluorinated material (ΔV = 171 mV), originate from the surface potential difference between alkylsilane and fluoroalkylsilane domains. An estimate of the surface potentials of the QDS and FAS layers based on the calculated dipoles of individual molecules (ODS – 1.18D and FAS – 1.47D) and their orientation gives a much stronger ΔV compared to the measured one. Therefore, several other factors such as intermolecular interactions, screening and depolarization effects should be considered for the rational interplay between the experimental and theoretical results.

There is a promise that KFM applications will also become important in studies of biological samples, yet applicability of this method in water solutions is not fully clarified. A condensation of dipalmitoylpho sphatidylcholine (DPPC) monolayer at the air-water interface in a Langmuir-Blodgett trough was monitored with KFM.[26] This process includes structural transitions from the expanded condition state to a mixture of liquid expanded (LE) and liquid condensed (LC) phases and, finally, to solid condensed (SC) state. The single layers, which were transferred to an Al-coated glass substrate, exhibit a surface potential ~270 mV higher than that of bare Al. Surface potential of the layers increases 50-100 mV on transition from LE to LC phase and 300 mV on transition from the LC to the SC state. The increase of molecular density was an adequate explanation of the changes of LE and LC potentials, whereas the steep potential raise in the SC phase resulted from a compression-induced change of the effective dipole near the polar head group of lipid molecules.

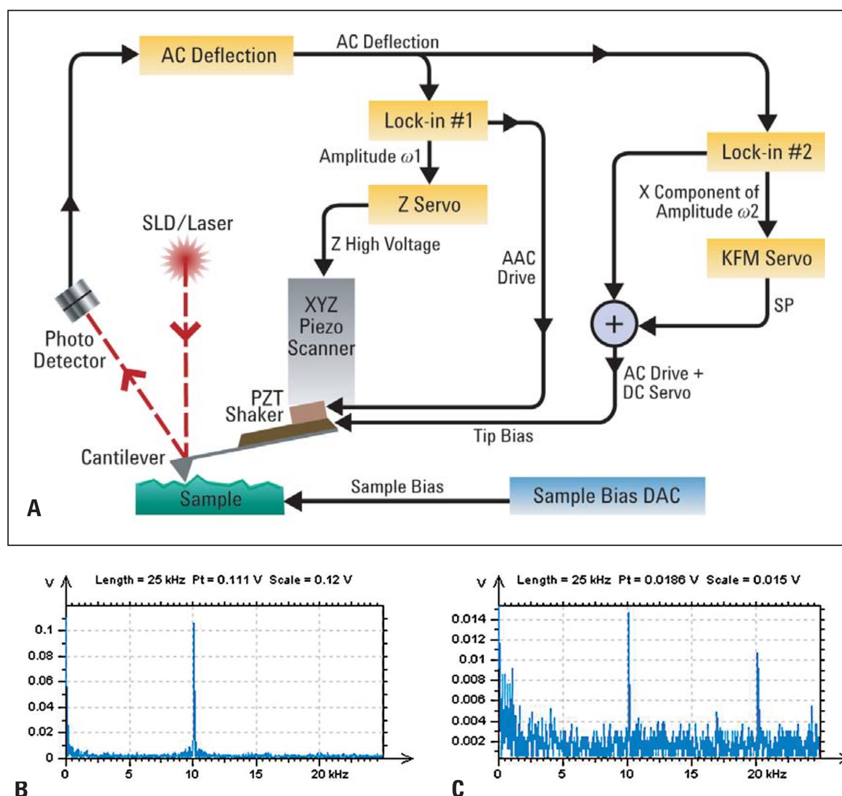

Figure 4A-C. A block-diagram of the implementation of KFM in Agilent 5500 scanning probe microscope using the MAC III accessory. (B)-(C) Amplitude-vs-frequency sweeps of LIA-2 signal (X-component of amplitude) with the electric servo loop in the "off" and "on" states, respectively.

KFM measurements with Agilent 5500 scanning probe microscope

There is no doubt that local measurements of the electrostatic force are among the most essential capabilities of a modern scanning probe microscope. The practical implementation of EFM and KFM in Agilent 5500 scanning probe microscope is enabled with the MAC III accessory, see the general set-up in Figure 4A. A sample on a microscope stage is grounded (or biased) and an electric signal is applied to a conducting probe. The probe oscillation, which is excited at or near its resonance ω_{mech}, changes its response to the tip-sample forces that is monitored with a photodetector. The photodetector output carrying the AC probe amplitude is sensed in parallel by LIA-1 and LIA-2. The LIA-1 is tuned to ω_{mech}, and it delivers the error amplitude signal ($A_i – A_{sp}$, where A_i – measured amplitude in a new surface location) to the servo that controls the vertical tip-sample separation. This servo loop is used for topography imaging. LIA-2 is tuned to ω_{elec} and from the input signal the X-component of amplitude at ω_{elec} is selected for servoing the tip voltage to nullify the incoming signal. In preparation for KFM imaging the phase of LIA-2 is tuned to maximize the X-component signal. The operation of the electric servo loop can be monitored and controlled with LIA-3, which sweeps the frequency around ω_{elec}. Typical sweep curves in the "on" and "off" states of the electric servo loop are shown in Figures 4B-C, where the scale is ~10× smaller in C. The detection of the amplitude signal at ω_{elec} = 10 kHz in the "off" state helps to optimize the experiment parameters, e.g. the level of AC voltage applied to the probe in the second loop. The MAC III accessory can provide a voltage up to ±10 volts, however the voltage should be chosen as small as possible to minimize its influence on the sample's electronic states. We have operated with the voltages in the 1-5 V range. In the "on" state one should minimize the remainder of the amplitude signal (the error signal in the feedback operation)

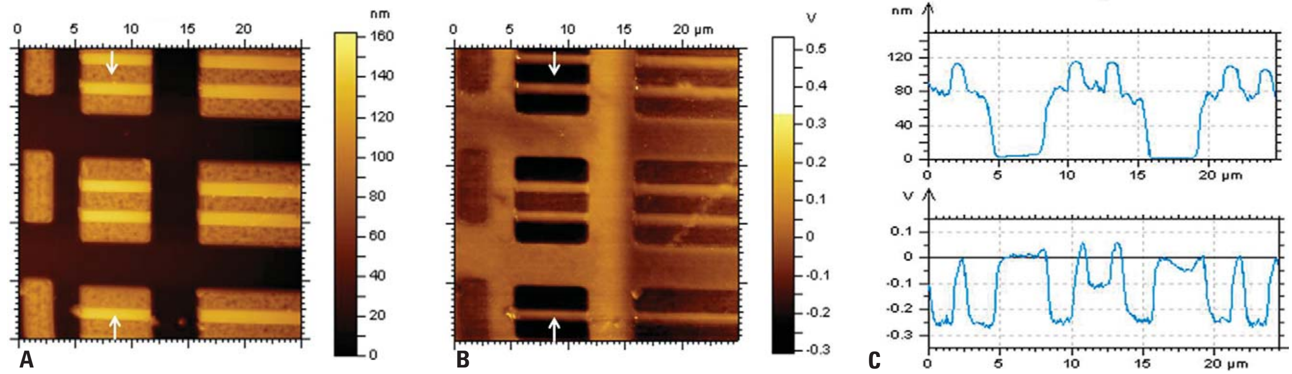

Figure 5A-C. The topography (A) and surface potential (B) images of SRAM. The cross-section profiles along the directions indicated with white arrows in (A) and (B) are shown in the top and bottom parts of (C).

at ω_{elec}=10 kHz by optimizing servo gain parameters. The experimental protocol for KFM also includes a compensation of the occasional contribution to surface potential measurements from the probe and sample surroundings; which causes a dependence of surface potential on the probe-sample separation. This dependence is eliminated by finding the proper offset voltage. The optimization procedures for KFM measurements are described in more detail in [27].

In the single-pass KFM experiment one needs to select ω_{mech} and ω_{elec}. A mechanical drive of the probe is typically done at ω_{mech} chosen near the first flexural resonance of the cantilever, whereas the electric servo loop is set either at much lower frequency or at the second or even third flexural mode. The following arguments are usually considered in the choice of ω_{elec}. The electrostatic probe response is higher at the resonant frequencies, yet this also increases the possibility the cross-talk between different force interactions. The cross-talk is less probable when $\omega_{elec} << \omega_{mech}$ but the probe response at non-resonant frequencies is also smaller. If the sensitivity is the real problem, then one can try to use the second flexural mode for ω_{mech} and first flexural mode for ω_{elec}. The particular choice of the frequencies is also related to the type of AFM probes used in KFM studies. For example, most of the measurements described in this paper were made with conducting Pt-coated Si probes (Olympus), which have a spring constant of 3-5 N/m and the resonance of the first flexural mode in the 60-80 kHz range. Low-frequency of 10 kHz and the second flexural mode of the probes (400-500 kHz) were most often chosen for ω_{elec}. TEM micrographs of these probes showed that their apex has a diameter of 20 nm or less.

In some cases, we also used the T-shaped Si probes (MikroMasch) with the tip being offset from the main cantilever axis. These probes exhibit pronounced torsional motion when the tip comes into interaction with the sample. The torsional resonant frequency (around 700 kHz) was successfully applied as ω_{elec} for KFM imaging of semifluorinated alkanes. It is worth noting that a doping level of these probes was sufficient enough to use them for electrostatic measurements without a conducting coating.

From the analysis of the KFM results it became clear that the operation in the non-contact regime substantially limits its spatial resolution, which is in the range of a few tens of nanometers. The remote positioning of the conducting probe while recording the electrostatic force response is also a feature of the lift mode. The only exception is the KFM measurements performed with FM mode in UHV, where the surface potential images made on atomically smooth surfaces demonstrated atomic-scale features.[28] However this mode is not very suitable for imaging at ambient conditions on corrugated surfaces. The examples of AM imaging in Figures 1A-H demonstrated that when the position of A_{sp} changed from the gradual sloped part of the AvZ curve to the steep one (in other words, from the non-contact operation to the intermittent contact regime) the topography image shows well-resolved surface features yet the electrostatic response was lost, most likely, due to the use of the same frequency: ω_{mech}. Therefore, it appears quite intriguing to perform the single-pass KFM measurements at ω_{mech} and ω_{elec} in the intermittent contact regime. One might expect that resolution of the electrostatic force detection in this operation will be improved while cross-talk between topography and the electrostatic force response might become evident. These features will be of concern in the analysis of KFM applications in the intermittent contact regime, which are shown below. Most of these images were obtained with A_0 = 10-15 nm and A_{sp} = 0.6A_0 – the parameters, which according to the AvZ curves are unambiguously related to the intermittent contact regime in a low-humidity environment (RH<20%) where the studies were performed.

KFM in the intermittent contact regime: Practical examples

The first two examples are taken from KFM studies of semiconductor samples: SRAM and a SiGe structure. The topography and surface potential images of the same sample regions show dissimilar patterns, Figures 5 and 6. The locations of different doping types and levels as well as few local defects visualized in surface potential images are clearly different from topographic features. This is confirmed by the cross-section profiles taken in the images along the directions marked with white arrows. Therefore, we conclude that the cross-talk between the topography and the probe response to the electrostatic forces is negligible. In the control experiments we obtained surface potential images of SRAM with different combinations of ω_{mech} and ω_{elec} (first flexural resonance/10 KHz, first flexural resonance/second flexural resonance; second flexural resonance/first flexural resonance). The comparison of the quantitative values in the surface potential profiles showed that the variations did not exceed 10%. As regarding the sensitivity of this approach, the variations as small as 10 mV are distinguished in the surface potential profiles, Figures 5C and 6C. It also noticeable that surface potential is substantially negative in the SRAM locations and around 0 in the SiGe

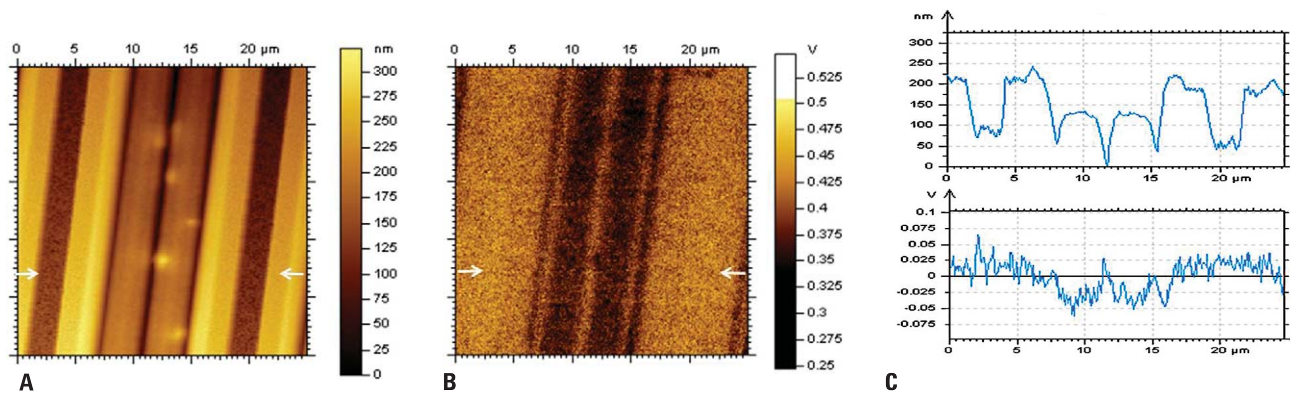

Figure 6A-C. The topography (A) and surface potential (B) images of a SiGe structure. The cross-section profiles along the directions indicated with white arrows in (A) and (B) are shown in the top and bottom parts of (C).

structure. In KFM of semiconductors a correlation between the surface potential as the probe location and surface Fermi level is established by a following equation:

(6) $E_{Fs} - E_{vac} - V_{probe} - \phi_p,$

where E_{Fs} - the surface Fermi level, E_{vac} – vacuum level, V_{probe} – surface potential measured by the probe, and ϕ_p – work function of the probe material. Therefore, evaluation of local surface Fermi level is a feasible task in KFM of semiconductor samples,[29] after a proper calibration of the probe, an appropriate sample preparation and thoroughly performed the experiments. These applications are beyond the scope of this paper.

In further evaluation of KFM operation we conducted experiments similar to those described in [10], which are often used for surface lithography.[30-31] In these experiments, surface charges were deposited by a tip-sample voltage discharge on surface of PMMA and normal alkane $C_{60}H_{122}$ layers on Si and graphite, respectively. The charges were deposited above the voltage threshold, which is around 5-10 V (depending on a layer thickness and annealing state), and a 2 msec pulse was used. The first pair of images in Figures 7A-B shows the PMMA topography and a circular surface charge pattern with maximum around 1.5 V. In this case, there is no discernible cross-talk between the charge and topography. The situation is different when a higher voltage impulse was applied, Figures 7C-D. The topography image exhibits a pattern of complex shape with negative and positive levels, thus demonstrating a strong involvement of the electrostatic forces in the tracking feedback when the local charge is large, Figure 7D. In other words, the large spatial dimensions and high

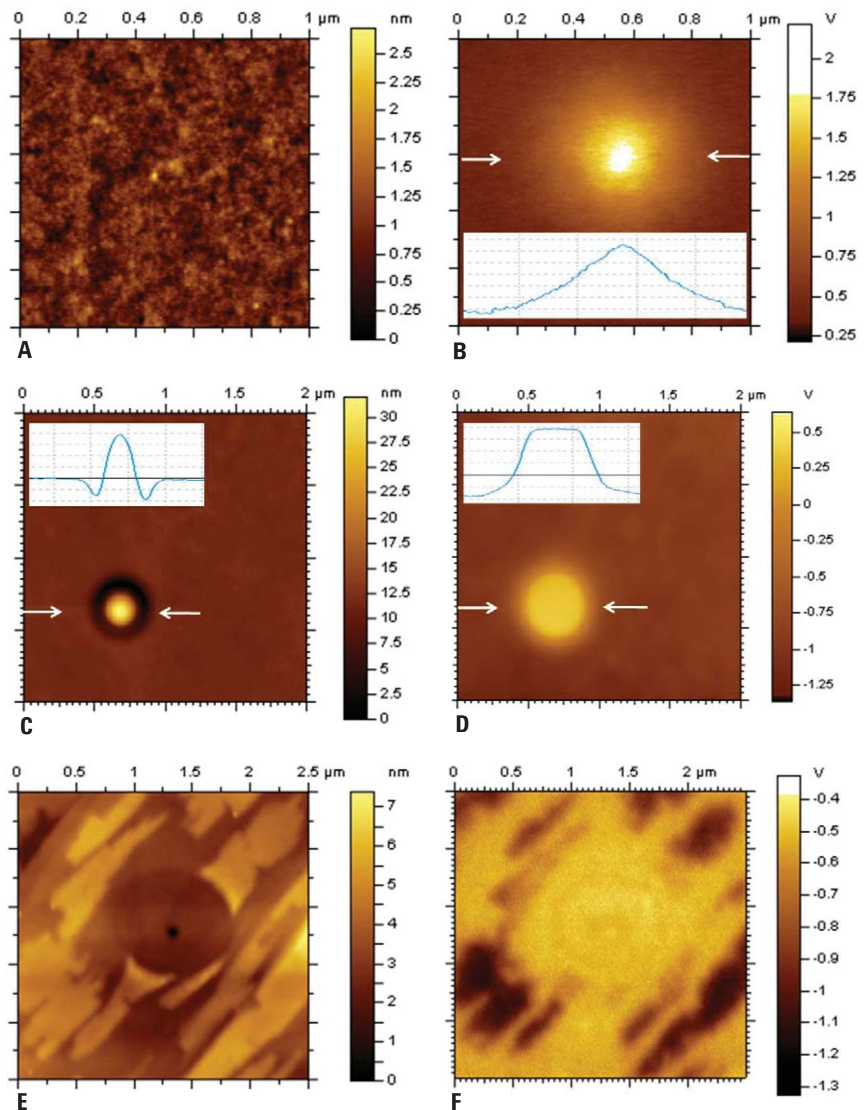

Figure 7A-F. The topography (A, C, E) and surface potential (B, D, F) images of PMMA layers on Si around the locations subjected to tip-voltage pulses. The inserts in the (B-D) show the cross-section profiles along the directions indicated with white arrows. (E) - (F) The topography and surface potential images of normal alkane $C_{60}H_{122}$ adsorbate on graphite around the location subjected to a tip-voltage pulse.

intensity of the generated charge makes its compensation by the probe voltage inefficient. AFM studies of ultrathin adsorbates of normal alkanes on graphite revealed that the alkanes form lamellar domains in which the chains are aligned parallel to the surface.[32] The voltage pulse applied to the $C_{60}H_{122}$ layer on graphite induced a circular damage pattern in the adsorbate and even in graphite substrate visible as a hole in the center. The surface potential shows a bright-contrast at the circular pattern, which can be assigned to the surface potential of the substrate. In addition, dark patterns surrounding the disk-like region represent the generated negative charges on the elevated alkane domains. The negative charges on the alkane domains have persisted for several days. Further high-resolution AFM images (not shown here) demonstrated that the lamellar order of the domains was destroyed and the material of the domains displays a granular morphology. Most likely, the discharge caused a variety of different chemical processes. Therefore, this approach can be applied not only for lithography but also for local initiation and monitoring of chemical reactions.

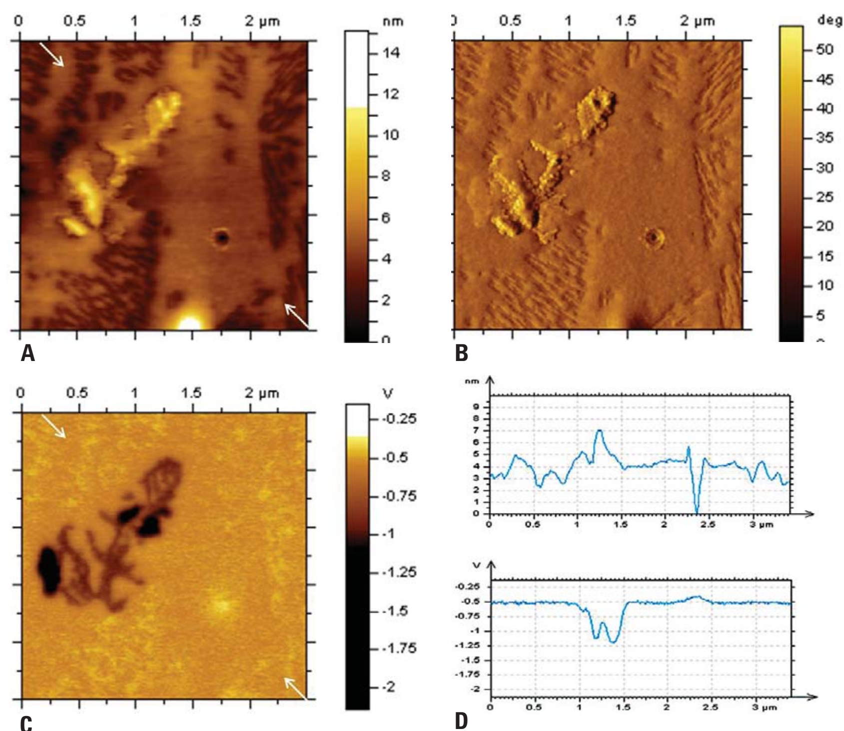

Figure 8A-D. The topography (A), phase (B) and surface potential (C) images of $F_{14}H_{20}$ adsorbate on graphite. The cross-section profiles taken along the directions shown with white arrows in (A) and (C) are presented in the top and bottom parts of (D), respectively.

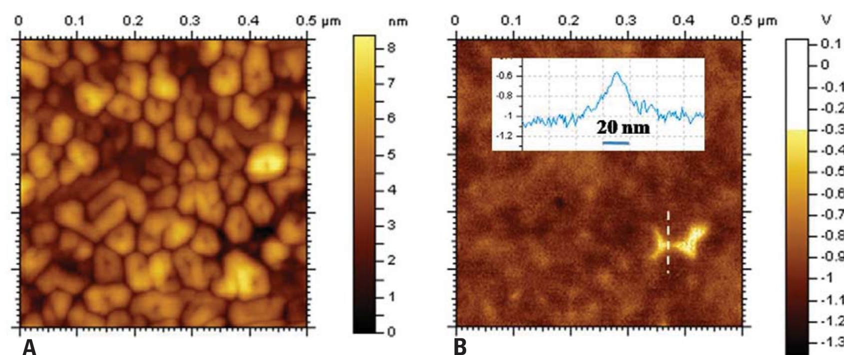

Figure 9A-B. The topography (A) and surface potential (B) images of $F_{14}H_{20}$ adsorbate on graphite. The insert in (B) shows a cross-section profile along the direction marked with a white dashed line.

The AM imaging of an adsorbate of semifluorinated alkanes $F_{14}H_{20}$ on graphite (Figures 2A-F) provides subtle clues of a negative charge on the self-assemblies, and these samples were examined with KFM. The topography, phase and surface potential images of this material are shown in Figures 8. The topography image reveals a brighter aggregate among patches of the featureless material lying on a thinner layer of $F_{14}H_{20}$, Figure 8A. A small hole with a tiny rim is seen in the bottom right part of the image. It was made by a tip voltage pulse and it was expected that the pulse will ablate the material and expose the graphite surface underneath. The phase image resolves fine structures in the aggregate, which are slightly brighter than the rest of the image, Figure 8B. Otherwise, the phase contrast is fairly homogeneous with the error-signal-like features at the edges of the patches and the hole. The surface potential image, which exhibits several levels of the contrast, is most informative, Figure 8C. First of all, the aggregate exhibits surface potential substantially more negative (up to -0.8 V) than that of the substrate seen at the location in the hole. This is best seen in Figure 8D, which presents the cross-section profiles taken along the directions indicated with white arrows in images A and C. The topography profile traversing the hole shows that the thickness of the patches is only few nanometers. Also, the very dark patches seen in the surface potential image of the aggregate suggest that its constituents might form structures with larger charge. Besides the aggregate and the hole, the contrast of the remainder of the image is more homogeneous with small variations between areas with the featureless adsorbate.

Self-assembly of $F_{14}H_{20}$ adsorbates results in nanoscale structures of different morphologies (toroids, ribbons, spirals and their intermediates) and various packing motifs[33] that make them attractive for a demonstration of KFM resolution. A region of $F_{14}H_{20}$ adsorbate on graphite, which is densely populated with deformed toroids and short ribbons, is shown in the topography image in Figure 9A. The

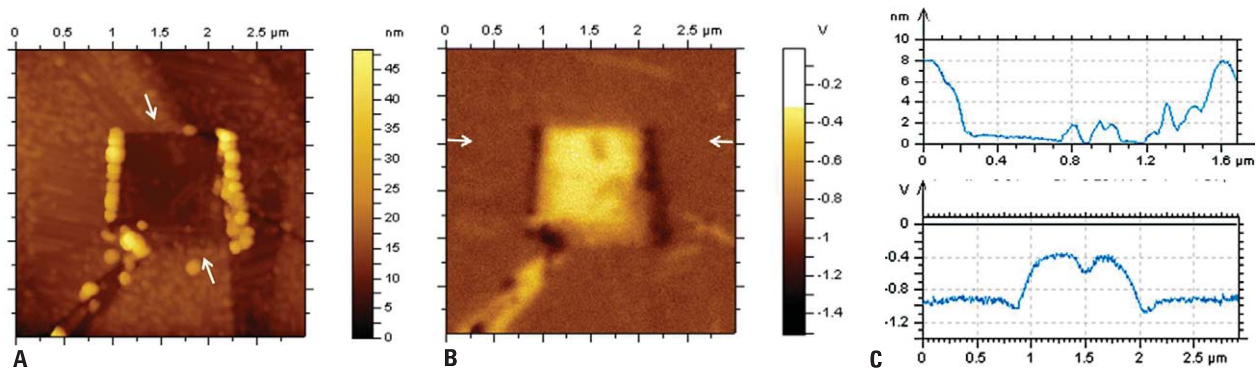

Figure 10A-C. The topography (A) and surface potential (B) images of $F_{14}H_{20}$ adsorbate on graphite in the area around the "window" made by the AFM tip scanning in the contact mode. The top and bottom graphs in (C) – show the cross-section profiles across this area in (A) and (B), which were taken along the directions marked with white arrows.

surface potential contrast of this area is not very pronounced, except for the bright spot seen at the location, which is closer to the substrate than the rest of the surface, Figure 9B. This is apparently a void in the packing of surface structures. The cross-section profile in the insert of the image indicates that the width of the void is less than 10 nm. This allows us to claim that the spatial resolution of KFM operating in the intermittent contact mode is better than 10 nm. The variations of the contrast between the different self-assembled structures (up to 0.2 V) are much smaller as compared to the 0.8 V average contrast between the void's location and the rest of the image. The fact that the void contrast is approximately that of the substrate is confirmed by the images and cross-section profiles shown in Figures 10A-C. The topography image in Figure 10A presents a larger area of the $F_{14}H_{20}$ adsorbate after its central part was removed from the substrate by mechanical abrasion (scanning of this location in the contact mode). This procedure, which is often applied for the evaluation of thickness of adsorbates on different substrates, is also useful in KFM analysis because it provides access to the substrate. The surface potential image in Figure 10B clearly demonstrates that the "window" is ~0.7 V higher in potential than the rest of the area. The images and the cross-section profiles in Figure 10C, which were taken along the directions marked with white arrows, show that the adsorbate is ~8 nm thick and that mechanical interference of the probe induced the formation of large micelles at the "window" edges and several ribbons inside the "window". Both the micelles and the ribbons are discernible in the surface potential image, where they are seen respectively darker and brighter than their immediate surroundings.

Up to this point, we have shown that KFM in the intermittent contact mode is not subject to noticeable cross-talk artifacts and provides sensitive imaging of surface potential with a spatial resolution of 10 nm or better. In studies of semifluorinated alkane $F_{14}H_{20}$, KFM distinctively differentiates material's features and ordered self-assemblies with the latter exhibiting negative surface potential. These applications were performed using the probe amplitude at ω_{elec} as a measure of electrostatically-induced tip-sample force interactions. Following the classification given in [34] we will use AM-AM abbreviation for this mode. This abbreviation indicates that AM is used in both feedback loops employed for topography tracking and electrostatic measurements. Another approach to KFM measurements and its use in the intermittent contact regime are introduced below.

KFM in AM-FM operation with Agilent 5500 microscope

The problem of sensitivity and spatial resolution in the AFM-based electrostatic measurements attracted increasing attention for several years. A thorough consideration of the imaging procedures, optimization of probe and data interpretation was given in [35]. The authors estimated the cantilever, tip cone and tip apex contributions to the electrostatic probe-sample force and force gradient and came to the conclusion that high spatial resolution can only be achieved when the tip-apex contribution is dominant. This condition can be realized by using probes with a special geometry (the probes with long and sharp tips) or by employment of force gradient detection. The other possibility – imaging at tip-sample distances smaller than 2 nm was expected to be difficult in practice. Higher spatial resolution and higher sensitivity in the force-gradient based KFM was shown in [36] – the paper, in which electrostatic force measurements in AM and FM detection schemes were critically analyzed. Particularly, the surface potential data obtained on a KCl sub-monolayer on Au (111) in FM nicely agree with results of ultraviolet photoelectron spectroscopy. Also in contrast to AM-detection, the surface potential measured with FM did not vary with probe-sample separations in the 30 nm range. The state-of-the-art EFM and KFM were presented in [34] where the AM-AM, FM-AM and FM-FM combinations used for such measurements were mentioned and briefly described. Surprising is the absence of the AM-FM combination despite the above considerations suggesting the high value of FM detection of electrostatic forces. We have implemented this capability in the Agilent 5500 microscope and critically evaluate this mode in studies of a variety of samples in the intermittent contact regime.

The block scheme of the AM-FM mode is presented in Figure 11A. The principal difference of this set-up with the one used for the AM-AM approach (Figure 4A) is that the input of LIA-2 is connected to LIA-1 for measuring the phase data at ω_{mech}. The phase changes are directly related to changes in the force gradient that defines AM-FM type studies. Practically, the AC voltage is applied to the probe at ω_{elec}, which should be within the bandwidth of the LIA-1. The probe response, at the mixed frequency, ω_{mech} and ω_{elec} is detected by LIA-2 and used for KFM feedback. The amplitude sweeps in the "off" and "on" states of the electric servo loop are presented in Figures 11B-C. The electrostatic forces between the cantilever and sample cause the cantilever to deflect at ω_{elec}, and at twice that frequency. The voltage modulation also causes a modulation of the force gradient which is greatest between the tip and the sample. These changing force gradient causes the resonant frequency of the cantilever to shift giving rise to side bands on the mechanical resonance of the cantilever. After demodulation by LIA-1, the output shows modulation at ω_{elec} and at twice that frequency. The two forms of KFM are similar in that the DC bias has a servo to minimize the ω_{elec} component from the input of LIA-2. The main differences between operation of AM-AM and AM-FM modes are related with choice of ω_{elec}, which in case of AM-FM is limited to low frequency (say 5kHz), low feedback gains of the electric servo loop and to lower AC voltages (usually much less than 1 V). The use of lower voltages is very positive remembering the possible voltage influence on sample surface electric properties.

There is another implementation of AM-FM combination in which the Y-vector of amplitude is used, instead of the phase signal of LIA-1. When the phase of LIA-1 is adjusted so the amplitude of the cantilever is aligned with the X-component then the tip-sample force interactions can be observed as the Y-component variations. The latter naturally reflect the phase signal, which is calculated using the X- and Y-component data. Therefore, for improved signal-to-noise ratio it might be worth using just the Y-component. Practically, with LIA-1 set to ω_{mech} one needs to maximize the X-component and make the Y-component close to zero. Then, the Y component should be directed to LIA-2 and the electric servo loop.

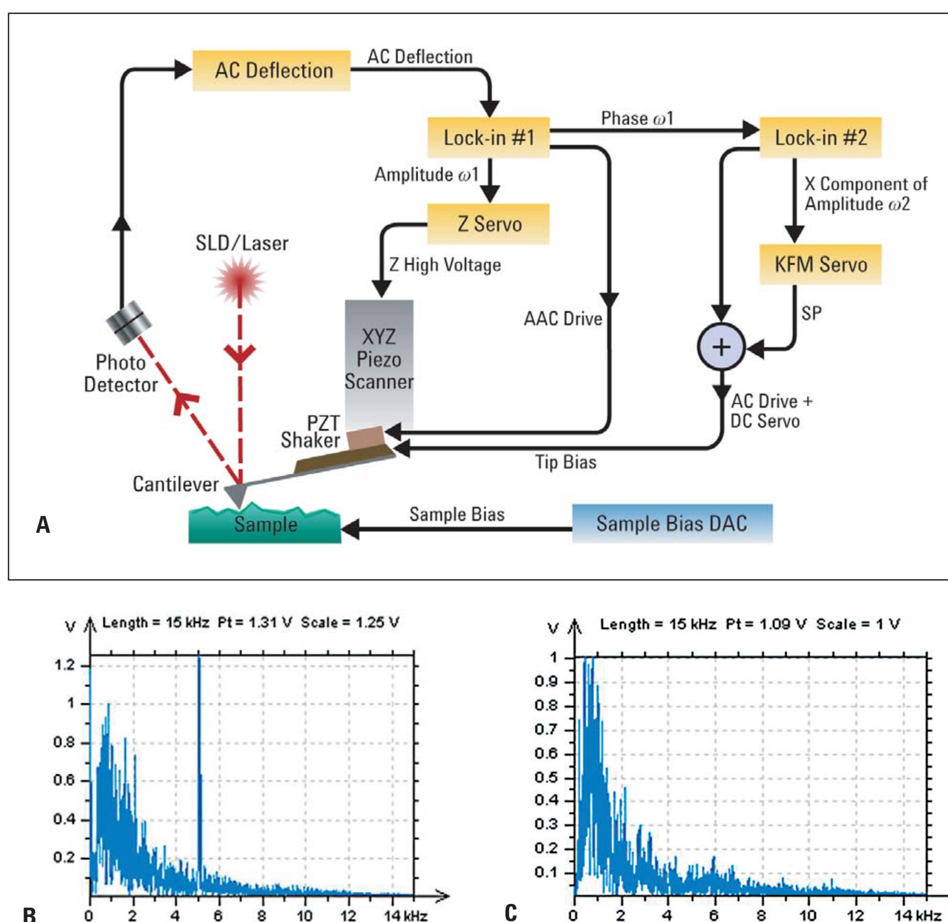

Figure 11A-C. A block-diagram of the implementation of KFM in Agilent 5500 scanning probe microscope using the MAC III accessory. (B)-(C) Amplitude-vs-frequency sweeps of LIA-2 signal (X-component of amplitude) with the electric servo loop in the "off" and "on" states, respectively.

KFM with AM-FM operation in the intermittent contact: Practical results

After implementation of AM-FM approach in KFM we have checked the value of the phase- and Y-component-based operations by comparing these modes and AM-AM approach in the intermittent contact imaging of $F_{14}H_{20}$ adsorbate, Figures 12A-E. The chosen sample of $F_{14}H_{20}$ adsorbate has many of heterogeneities due to partial self-assembly of the material into individual micelles and their aggregates. As expected from our AM-AM studies the self-assemblies exhibits strong surface potential contrast what indeed is noticed in the images obtained with all three modes, Figures 12B-D. The comparison of the images and also the surface potential profiles shown in Figure 12E demonstrates the favorability of AM-FM approaches in studies of semifluorinated alkanes. The images in Figures 12C-D exhibit higher contrast, and therefore resolution than the image in Figure 12B. Particularly, a visualization of the patches in the top right parts of the images is the best illustration. The cross-section profiles also show that the values of the surface potential are higher in AM-FM modes compared to the AM-AM. As expected the surface potential signal obtained with the phase-based and Y-component-based operations are quantitatively the same but the signal-to-noise ratio is definitely improved in the Y-component-based operation. Most likely the values of the surface potential in the 0-1.0 V range obtained in the AM-FM studies are defining surface charges more precisely than the potential data obtained in the AM-AM operation similar to the findings in [36].

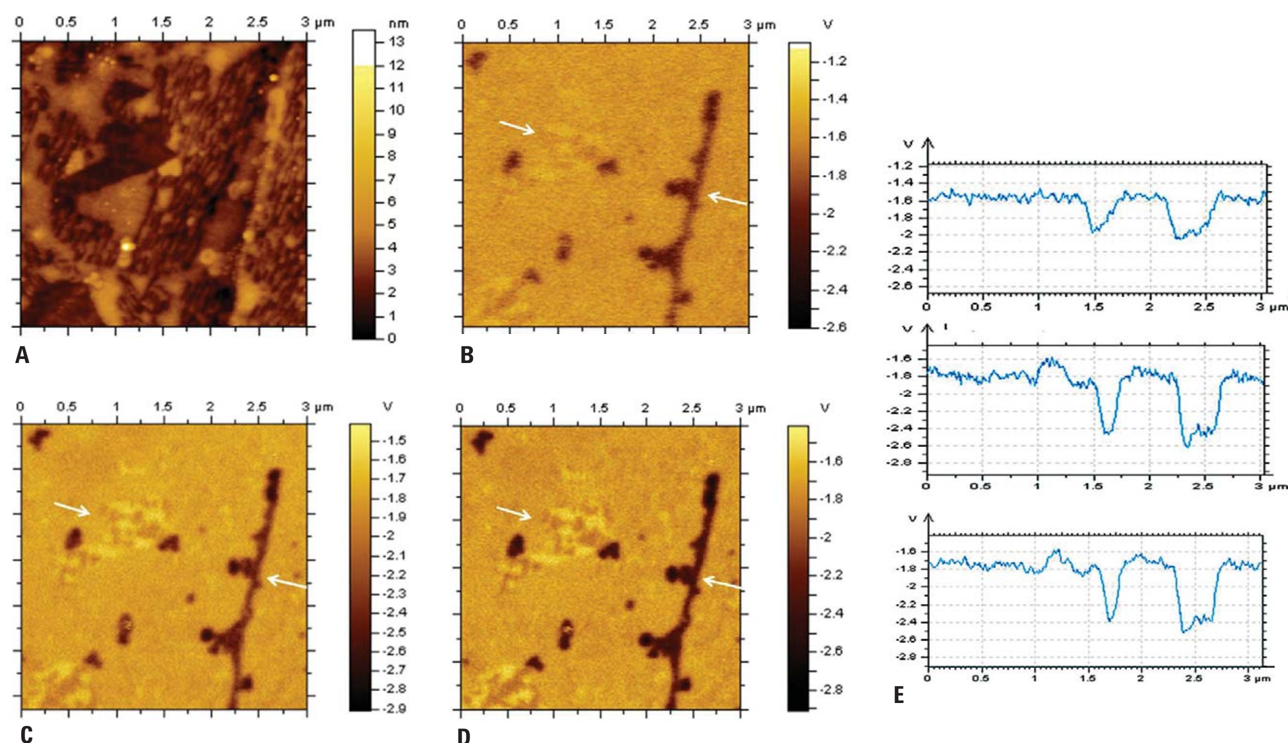

Figures 12A-E. The topography (A) and surface potential (B) images of $F_{14}H_{20}$ adsorbate on graphite obtained in the AM-AM operation. (C)-(D) Surface potential images of the same location as in (A) and (B) obtained in AM-FM operation with the phase and the Y-component signals for the electric servo loop. (E) The cross-section profiles taken along the direction indicated with white arrows in (B) – top, (C) – middle, (D) – bottom.

In an attempt to determine the spatial resolution of KFM in the AM-FM operation we further examined $F_{14}H_{20}$ adsorbates at scales of 1 micron and smaller, and the results, which were obtained in the phase-based AM-FM operation, are collected in Figures 13 and 14. The images in Figures 13A-D show an aggregate of self-assembled structures and a single toroid less than 50 nm in diameter. As expected the aggregate, which consists of a number of toroids and other elementary self-assemblies exhibits strong negative contrast (~-1.0V) even larger than that of the toroid (~-0.8V). Remarkably, the other adsorbate patches being of comparable size and height to the self-assembled aggregate do not exhibit any noticeable variations of surface potential. The toroid, which is presented in the images in Figures 13C-D, has a height of ~3.2 nm and surface potential of ~0.8 V. The latter is consistent with surface potential of a Langmuir-Blodgett layer of similar compound determined with a macroscopic Kelvin probe.[37] The toroid is most likely formed of extended molecules (contour length 4.6 nm) with fluorinated groups pointed away from the surface. At the toroid edges, the hydrocarbon segments are bending towards the surface to compensate the mismatch of electron density in the hydrocarbon and fluorinated structures. Therefore, the $–CF_2-CH_2-$ dipole orientation towards the substrate is primarily responsible for the surface charges observed in KFM. Self-assemblies of $F_{14}H_{20}$ and other semifluorinated alkanes F_nH_m have been under examination for some time. Despite the fact that a number of techniques (X-ray reflectivity, AFM, surface IR techniques and a macroscopic Kevin probe) were applied to examination of molecular arrangements in these nanostructures their molecular architecture is still not clarified.[38-40] In the ongoing KFM studies of $F_{14}H_{20}$ and related compounds we examined their self-assemblies on different substrates and in different environments in pursuit of a better understanding of their structures and behavior.[41]

As regarding the KFM resolution we point out fine features in the sub-10 nm range, which were observed in the topography and surface potential images of the $F_{14}H_{20}$ adsorbate, Figures 14A-C. This area is filled by the toroids and self-assembled ribbons. The surface potential of the

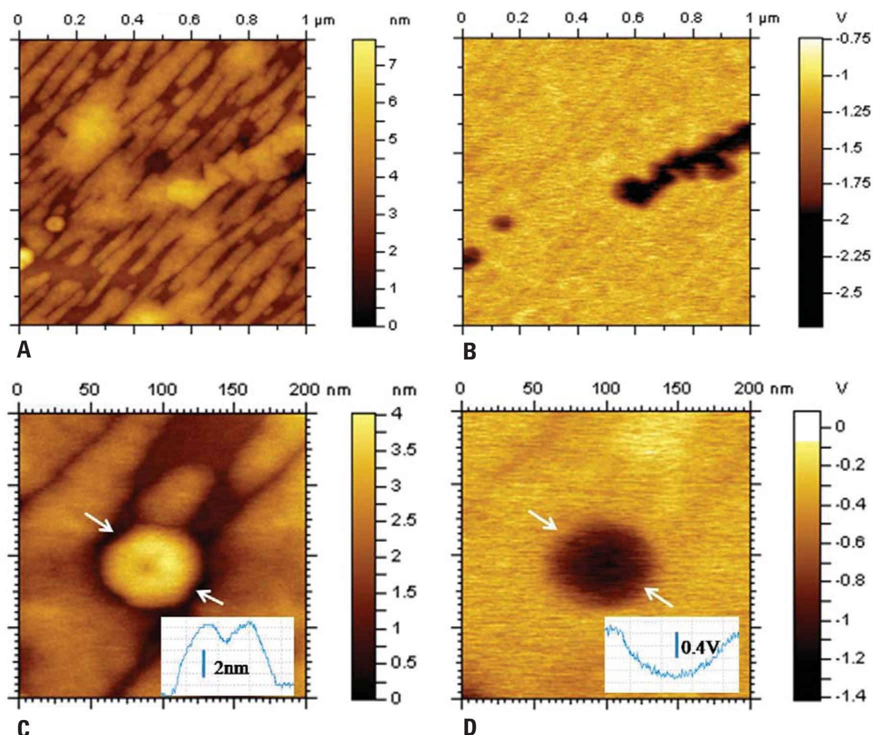

Figures 13A-D. The topography (A, C) and surface potential (B, D) images of $F_{14}H_{20}$ adsorbate on graphite obtained in the AM-FM operation. The inserts in (C-D) show the cross-section profiles taken along the directions indicated with white arrows.

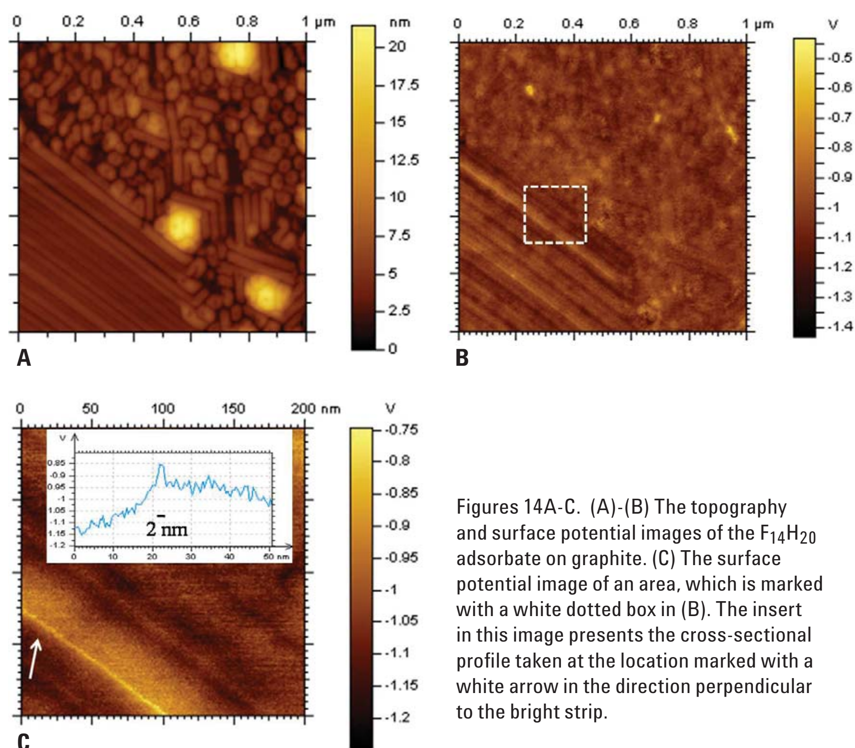

Figures 14A-C. (A)-(B) The topography and surface potential images of the $F_{14}H_{20}$ adsorbate on graphite. (C) The surface potential image of an area, which is marked with a white dotted box in (B). The insert in this image presents the cross-sectional profile taken at the location marked with a white arrow in the direction perpendicular to the bright strip.

ribbons is only slightly different from that of the toroids, similar to the observations in Figure 8B. Nevertheless, there are few locations with very pronounced contrast: the voids between the toroids and the slits between the ribbons. At these locations the probe "feels" the substrate better than elsewhere. The high-resolution surface potential images of the area outlined with a red dotted square is given in Figure 14C. The insert shows the profile across one of the slits in the location pointed with a white arrow. The width of the 0.1 V peak seen in this profile is around 2 nm that can be used as a measure of spatial resolution of KFM AM-FM operation in the intermittent contact mode. This result suggests that the sensing apex area of the AFM probe, which is much smaller than the tip diameter (~20 nm), dominates in the electrostatic measurements. The achieved high-resolution is in line with the expectation of [35] where the force-gradient detection combined with a small tip-sample distance was advocated as a way to enhance resolution. The use of sharper conducting probes might help to increase the resolution further.[42]

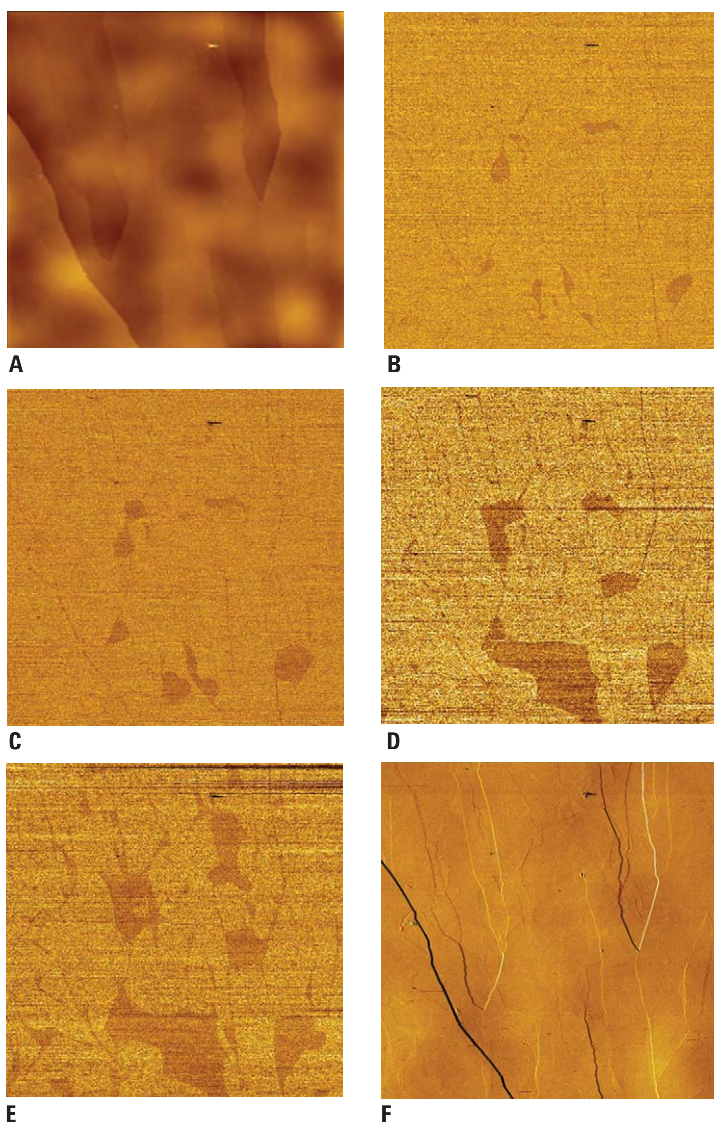

Figures 15A-F. (A -(B) The topography and surface potential images of graphite 2 hr after cleavage. (C)-(D) The surface potential images of graphite 2.25 and 2.5 hr after the cleavage. (E)-(F) The surface potential images of graphite 2.75 hr after cleavage. Scan size: 20 µm.

In exploring the use of KFM for the mapping of surface heterogeneities we conducted long-term imaging of a freshly-cleaved sample of graphite. Several images of the series are documented in Figures 15A-F. The topography and surface potential images taken 2 hours after the cleavage show a surface region with several steps of graphite planes (Figure 15A) and few dark patches with different potential. Such patches were not seen at shorter times after the cleavage and, therefore, they are assigned to air-borne contamination deposited on the surface. As time progresses, these patches increased in size, and new patches originated as well. This process is visible in the images in Figures 15C, D, E, which were recorded in 15 minutes intervals after the ones in Figures 15A-B. The difference of the potentials of the fresh and contaminated surfaces was ~ 60 mV and did not change as the contamination grows. At longer times the contamination has covered the entire area and the surface potential image becomes homogeneous again. Remarkably, phase images were not as sensitive to the growing contamination as the surface potential images. The phase image in Figure 15F is the first in which the patches became distinguishable. The simultaneously recorded surface potential image revealed the contamination areas in more pronounced way, Figure 15E. KFM images of freshly prepared Au (111) also showed a contamination traces at the edges of gold terraces.[43] Our data demonstrate the high-sensitivity of KFM to the air-borne contamination of the substrates often used in AFM. These results should be considered by researchers using these substrates.

As the final example of KFM capabilities we chose the images of $F_{14}H_{20}$ adsorbate on Si substrate (Figures 16A-F), which were collected when the sample was held in humid atmosphere in the environmental chamber of an Agilent 5500 microscope. The experiments lasted over two days, and the changes in surface topography that happened after the first 24 hours are shown in Figures 16A-B. Three domains consisting of spiral self-assemblies have substantially expanded in the lateral dimensions as evidenced by the reference positions of two contamination features indicated with white arrows. The spiral self-assemblies loosen their initial tight packing inside the domains and the individual spirals became well-separated from their neighbors as clearly seen in Figure 16C. Three factors should be considered in the tentative explanation of this observation. They include the negative charge of individual spirals, an influence of humidity on their adhesion to the substrate and the possible tip-force involvement in the spirals' motion. More changes occurred after the 48 hours exposure of the sample to humid environment as many spirals have converted into individual toroids, Figures 16C-D. Surprisingly, this process, which was noticed in vapors of organic solvents,[32] can also take place in a humid atmosphere. The topography and surface potential images of an array of $F_{14}H_{20}$ toroids are shown in Figures 16E-F. The surface potential of the toroids in humid air (-0.4 V) is much smaller than in dry air. One might suspect a partial shielding of surface charges similar to the non-contact KFM observations of semiconductor samples.[44] However, this effect is expected to be less when KFM studies are performed in the intermittent contact regime. This problem will be further explored.

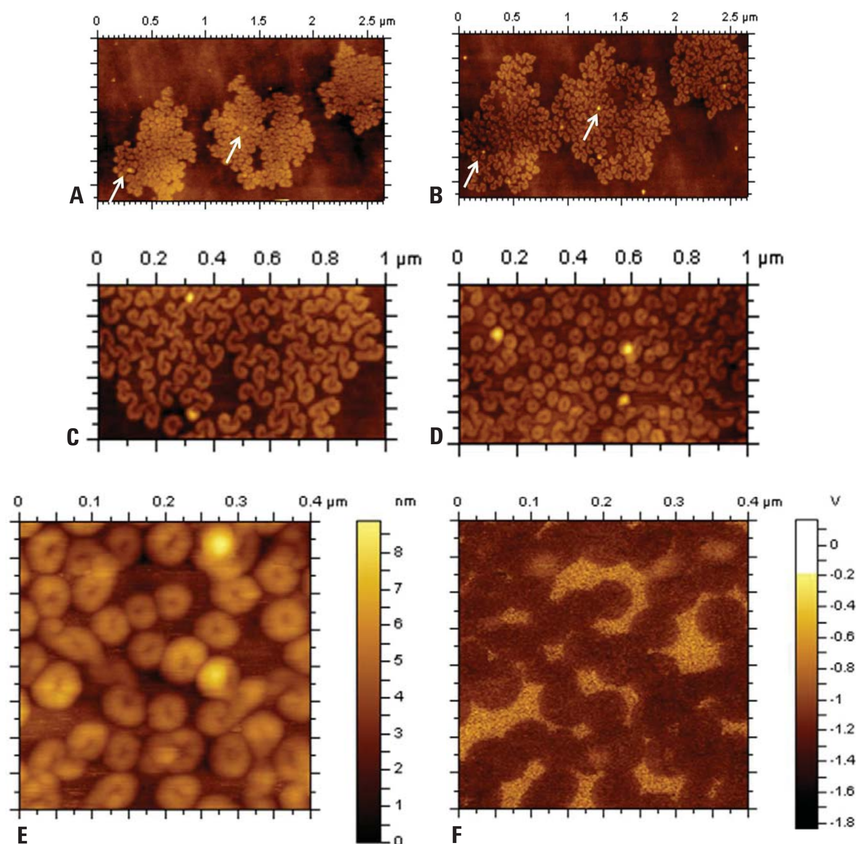

Figures 16A-F. (A)-(B) The topography images of $F_{14}H_{20}$ adsorbates on Si substrate after the sample was placed in humid air and after 24 hr exposure to humid air, respectively. (C)-(D) The topography images of $F_{14}H_{20}$ adsorbates on Si substrate after 24 hr and 48 hr exposure to humid air, respectively. (E)-(F) The topography and surface potential images of the sample shown in (D). All images were collected in humid air.

Conclusions

This paper describes KFM operations using an Agilent 5500 scanning probe microscope enhanced with a MAC III accessory that allows multi-frequency AFM measurements with 3 dual phase lock-in amplifiers. Instrumental set-ups allowing force- and force-gradient-based KFM studies (AM-AM and AM-FM) are described and the value of these approaches is verified in studies of the doped areas of semiconductor samples, surface charges created on organic layers by voltage discharge, the contamination traces on graphite and self-assemblies of semifluorinated alkanes $F_{14}H_{20}$ on graphite and Si substrates in dry and humid air. The novelty of these applications is that they were performed in the intermittent contact regime and the AM-FM combination was introduced. The simultaneous and independent measurements of sample topography and surface potential (as small as 10 mV) were successfully demonstrated in these single-pass KFM studies. The comparative studies of $F_{14}H_{20}$ self-assemblies with AM-AM and AM-FM demonstrated that the AM-FM operation provide higher and, likely more accurate values of surface potential of these nanostructures. Remarkably, the AM-FM approach in the intermittent contact mode led to high-resolution surface potential measurements where the 2-nm wide features were clearly resolved. We undertook only the first steps in the practical evaluation of new capabilities offered by KFM studies and there are several opened questions to clarify. They include finding of ways of reproducible and precise measurements of surface local work functions, development of better probes that are fully conducting with 1 nm apex size, expanding KFM measurements to different environments and various temperatures and others. Furthermore, the discussed results were obtained in the intermittent contact mode at relatively small tip-sample interactions when phase images do not exhibit the pronounced contrast related to variations of local mechanical properties. It might be quite informative to perform KFM imaging at elevated tip-sample force, i.e. in the repulsive force regime to get simultaneously topography and maps of local electric and mechanical properties as was recently suggested.[45]

Acknowledgements

We are thankful to Prof. M. Moeller (RWTH, Aachen, Germany) for providing us with a sample of semifluorinated alkane, $F_{14}H_{20}$. The sample of $LiNbO_3$ with Ag particles is a kind gift from the laboratory of R. Nemanich (ASU, Tempe, AZ, USA).

References

1. G. Binnig, C.F. Quate, and Ch. Gerber "Atomic force microscope" *Phys. Rev. Lett.* **1986,** *56,* 930-933.

2. Y. Martin, C.C. Williams, and H.K. Wickramasinghe "Atomic force microscope-force mapping and profiling on a sub 100-Å scale" *J. Appl. Phys.* **1987,** *61,* 4723-4729.

3. Q. Zhong, D. Innis, K. Kjoller, V. Elings "Fractured Polymer/Silica Fiber Surface Studied by Tapping Mode Atomic Force Microscopy" *Surf. Sci. Lett.* **1993,** *290,* L688-L692.

4. T. Albrecht, P. Gruetter, D. Horne, and D. Rugar "Frequency modulation detection using high-Q cantilevers for enhanced force microscopy sensitivity" *J. Appl. Phys.* **1991,** *61,* 668-673.

5. T. Fukuma, T. Ichii, K. Kobayashi, H. Yamada, and K. Matsushige "True-molecular resolution imaging by frequency modulation atomic force microscopy in various environments" *Appl. Phys. Lett.* **1995,** *86,* 034103-034105.

6. S. Magonov "AFM in Analysis of Polymers" in *Encyclopedia of Analytical Chemistry,* (R. A. Meyers, Ed.), pp. 7432-7491, John Willey & Sons Ltd., Chichester, **2000.**

7. M. Bai, S. Trogisch, S. Magonov, and H. Taub "Explanation and correction of false step heights in amplitude modulation atomic force microscopy measurements on alkane films" *Ultramicroscopy,* **2008,** *108,* 946-952.

8. V.B. Elings, and J.A. Gurley "Scanning probe microscope using stored data for vertical probe positioning" US Patent 5,308,974, **1994.**

9. Y. Martin, D.A. Abraham, and H. K. Wickramasinghe "High-resolution capacitance measurement and potentiometry by force microscopy" *Appl. Phys. Lett,* **1988,** *52,* 1103-10005.

10. J.E. Stern, B.D. Terris, H.J. Mamin, and D. Rugar "Deposition and imaging of localized charge on insulator surfaces using a force microscope" *Appl. Phys. Lett.,* **1988,** *53,* 2717-2719.

11. B.D. Terris, J.E. Stern, D. Rugar, and H.J. Mamin "Localized charge force microscopy" *J. Vac. Sci. Technol.* **1990,** *A8,* 374-377.

12. T. Ohta, Y. Sugawara, and S. Morita "Feasibility study on a Novel Type of Computerized Tomography Based on Scanning Probe Microscope" *Jpn. J. Appl. Phys.* **1996,** *35,* L1222-L1224.

13. J.M.R. Weaver and D.W. Abraham, "High-resolution atomic force microscopy potentiometry" *J. Vac. Sci. Techn.* **1991,** *B9,* 1559-1561.

14. M. Nonnenmacher, M.P. O'Boyle, and H.K. Wickramasinghe "Kelvin probe force microscopy" *Appl. Phys. Lett.* **1991,** *58,* 2921-2923.

15. H. Yokoyama and M.J. Jeffery "Imaging high-frequency dielectric dispersion of surfaces and thin films by heterodyne force-detected scanning Maxwell stress microscopy" *Colloids Surf. A* **1994,** *93,* 359-373.

16. M. Fujihira "Kelvin probe force microscopy of molecular surfaces" *Annu. Rev. Mater. Sci.* **1999,** *29,* 353-380.

17. M. Luna, D.F. Ogletree, and M. Salmeron "A study of the topographic and electric properties of self-assembled islands of alkysilanes on mica using a combination of non-contact force microscopy techniques" *Nanotechnology* **2006,** *17,* S178-S184.

18. L. Buergi, H. Sirringhaus, and R.H. Friend "Noncontact potentiometry of polymer field-effect transistors" *Appl. Phys. Lett.* **2002,** *80,* 2913-2916.

19. K.P. Puntambekar, P.V. Pesavento, and C.D. Friesbie "Surface potential profiling and contact resistance measurements on operating pentacene thin-film transistors by Kevin probe microscopy" *Appl. Phys. Lett.* **2003,** *83,* 5539-5541.

20. M. Chiesa, L. Buergi, J.-S. Kim, R. Shikler, R.H. Friend and H. Sirringhaus "Correlation between surface photovoltage and blend morphology in polyfluorene-based photodiodes" *Nano Letters* **2005,** *5,* 559-563.

21. T. Glatzel, H. Hoppe, N.S. Sariciftci, M.Ch. Lux-Steiner, and M. Komiyama "Kelvin probe force microscopy study of conjugated polymer/fullerene organic solar cells" *Jpn. J. Appl. Phys.* **2005,** *44,* 5370-5373.

22. O.A. Semenikhin, L. Jiang, K. Hashimoto, and A. Fujishima "Kelvin probe force microscopic study of anodically and cathodically doped poly-3-methylthiophene" *Synthetic Metals* **2000,** *110,* 115-222.

23. E. Perez-Garcia, J. Abad, A. Urbina, J. Colchero, and E. Palacios-Lidon "Surface potential domains on lamellar P3OT structures" *Nanotechnology* **2008,** *19,* 065709 (6).

24. M. Fujihira, and H. Kawate "Scanning surface potential microscope for characterization of Langmuir-Blodgett films" *Thin Solid Films* **1994**, *242,* 163-169.

25. H. Sugimura, K. Hayashi, N. Saito, O. Takai, and N. Nakagiri "Kelvin probe force microscopy images of microstructured organosilane self-assembled layers" *Jpn. J. Appl. Phys.* **2001,** *40,* 4373-4377.

26. T. Inoue, and H. Yokoyama "Imaging of surface electrostatic features in phase-separated phospholipid monolayers by scanning Maxwell stress microscopy" *J. Vac. Sci. Technol. B* **1994,** *12,* 1569-1571.

27. J. Alexander, S. Magonov, Technical Support Note, Agilent, Chandler AZ, **2008.**

28. S. Kitamura, K. Suzuki, M. Iwatsuki, and C.B. Mooney "Atomic-scale variations in contact potential difference on Au/Si(111) 7×7 surface in ultrahigh vacuum" *Appl. Surf. Sci.* **2000,** *157,* 222-227.

29. T. Matsukawa, S. Kanemaru, M. Masahara, M. Nagao, H. Tanoue, and J. Itoh "Doping diagnosis by evaluation of the surface Fermi level using scanning Maxwell-stress microscopy" *Appl. Phys. Lett.* **2003,** *82,* 2166-2168.

30. P. Mesquida, and A. Stemmer "Attaching Silica Nanoparticles from Suspension onto Surface Charge Patterns Generated by a Conductive Atomic Force Microscope Tip" *Adv. Mater.* **2001,** *13,* 1395-1398

31. R.V. Martinez, N.S. Losilla, J. Martinez, Y. Huttel, and R. Garcia "Patterning Polymeric Structures with 2 nm Resolution at 3 nm Half Pitch in Ambient Conditions" *Nano Letters* **2007,** *7,* 1846-1850.

32. S.N. Magonov, and N. Yerina "High Temperature Atomic Force Microscopy of Normal Alkane $C_{60}H_{122}$ Films on Graphite" *Langmuir* **2003,** *19,* 500-504.

33. A. Mourran, B. Tartsch, M. Gallyamov, S. Magonov, D. Lambreva, B.I. Ostrovskii, I.P. Dolbnya, W.H. de Jeu, and M. Moeller "Self-assembly of the perfluoroalkyl-alkane $F_{14}H_{20}$ in ultrathin films" *Langmuir* **2005,** *21,* 2308-2316.

34. M. Nakamura, and T. Yamada in *"Roadmap 2005 of Scanning Probe Microscopy"* ed. S. Morita, Ch.6 *"Electrostatic Force Microscopy"* pp. 43-51, Springer, (Springer, Berlin, **2006**).

35. J. Colchero, A. Gil, A.M. Baro "Resolution enhancement and improved data interpretation in electrostatic force microscopy" *Phys. Rev. B* **2001,** *64,* 245403 (11).

36. U. Zerweck, CH. Loppacher, T. Otto, S. Grafstroem, and L.M. Eng "Accuracy and resolution limits of Kelvin probe force microscopy" *Phys. Rev. B* **2005,** *71,* 125424 (10).

37. A. El Abed, M-C. Faure, E. Pouzet, and O. Abilon "Experimental evidence for an original two-dimensional phase structure: An antiparallel semifluorinated monolayer at the air-water interface" *Phys. Rev. E* **2002,** *5,* 051603 (4).

38. T. Kato, M. Kameyama, M. Eahara, and K. Iimura "Monodisperse Two-Dimensional Nanometer Size Clusters of Partially Fluorinated Long-Chain Acids" *Langmuir* **1998,** *14,* 1786-1798.

39. Y. Ren, K. Iimura, A. Ogawa, and T. Kato "Surface micelles of $CF_3(CF_2)_7(CH_2)_{10}COOH$ on aqueous La3+ subphase investigated by atomic force microscopy and infrared spectroscopy" *J. Phys. Chem. B* **2001,** *105,* 4305-4312.

40. M. Maaloum, P. Muller, and M.P. Krafft "Monodisperse surface micelles of nonpolar amphiphiles in Langmuir monolayers" Angew. *Chem.* **2002,** *114,* 4507-4510.

41. J. Alexander, S. Magonov, M. Moeller "Topography and Surface Potential in Kelvin Force Microscopy of Perfluoroalkyl Alkanes Self-Assemblies" *JVST,* **2008,** submitted.

42. M. Zhao, V. Sharma, H. Wei, R.R. Birge, J.A. Stuart, F. Papadimitrakopoulos and B.D. Huey "Ultrasharp and high aspect ratio carbon nanotube atomic force microscopy probes for enhanced surface potential imaging" *Nanotechnology* **2008,** *19,* 235707 (7)

43. J. Alexander, and S. Magonov "Exploring organization of amphiphilic compounds with atomic force microscopy" Proceedings of X. Annual AFM Winter Workshop, Linz, **2008,** in press.

44. H. Sugimura, Y. Ishida, K. Hayashi, O. Takai, and N. Nakagiri "Potential shielding by the surface water layer in Kelvin probe force microscopy" *Appl. Phys. Lett.* **2002,** *80,* 1459-1461.

45. R.W. Stark, N. Naujoks, and A. Stemmer "Multifrequency electrostatic force microscopy in the repulsive regime" *Nanotechnology* **2007,** *18,* 0655023 (7).

AFM Instrumentation from Agilent Technologies

Agilent Technologies offers high-precision, modular AFM solutions for research, industry, and education. Exceptional worldwide support is provided by experienced application scientists and technical service personnel. Agilent's leading-edge R&D laboratories are dedicated to the timely introduction and optimization of innovative and easy-to-use AFM technologies.

www.agilent.com/find/afm

www.agilent.com

For more information on Agilent Technologies' products, applications or services, please contact your local Agilent office. The complete list is available at:
www.agilent.com/find/contactus

Phone or Fax

United States:	(tel) 800 829 4444 (fax) 800 829 4433
Canada:	(tel) 877 894 4414 (fax) 800 746 4866
China:	(tel) 800 810 0189 (fax) 800 820 2816
Europe:	(tel) 31 20 547 2111
Japan:	(tel) (81) 426 56 7832 (fax) (81) 426 56 7840
Korea:	(tel) (080) 769 0800 (fax) (080) 769 0900
Latin America:	(tel) (305) 269 7500
Taiwan:	(tel) 0800 047 866 (fax) 0800 286 331

Other Asia Pacific Countries:
tm_ap@agilent.com
(tel) (65) 6375 8100
(fax) (65) 6755 0042

Product specifications and descriptions in this document subject to change without notice.

© Agilent Technologies, Inc. 2008

Printed in USA, December 15, 2008
5989-9740EN

Agilent Technologies